Visualization of Orbits and Pattern Evocation for the Double Spherical Pendulum

Jerrold E. Marsden*
Control and Dynamical Systems,
California Institute of Technology, Pasadena, CA 91125.

Jürgen Scheurle†
Institut für Angewandte Mathematik
Bundesstrasse 55, D-20146 Hamburg, Germany

Jeffrey M. Wendlandt
Mechanical Engineering, University of California, Berkeley, CA 94720

April, 1995; this version: August 2, 1995

Proceedings of the ICIAM Conference, Hamburg, July, 1995

Abstract

This paper explores pattern evocation and the visualization of orbits of the double spherical pendulum. Pattern evocation is a phenomenon where patterns emerge when the flow of a dynamical system is viewed in a frame that rotates relative to the inertial frame. The paper begins with a summary of the theory on pattern evocation for mechanical systems with symmetry. The result of this theory is that if the motion in the reduced space is periodic (respectively, quasiperiodic or almost periodic), then when viewed in a suitably chosen rotating frame with constant velocity, the motion in the unreduced space is periodic (respectively, quasiperiodic or almost periodic). The motion of the system viewed in this rotating frame may have a particular pattern or symmetry. Examples of this theory are demonstrated for the double spherical pendulum. A differential-algebraic model is created for the double spherical pendulum and is integrated with the simulation package MEXX as well as a custom energy-momentum integrator.

*Research partially supported by NSF, DOE, and NATO.
†Research partially supported by DFG and NATO.

Contents

1 Introduction **3**

2 Summary of the Theory on Pattern Evocation **3**
2.1 Uniform Frames for Equivariant Dynamical Systems 3
2.2 Symplectic Reduction 3
2.3 Cyclic Coordinates and the Frame Angular Velocity Formula 4
2.4 Quasiperiodic Orbits 4
2.5 Discrete Symmetries 5

3 The Double Spherical Pendulum System **6**
3.1 The Configuration Space, Lagrangian and Hamiltonian 6
3.2 Symmetries 7
3.3 The Reduced Variables 7

4 Simulation Results and Patterns **8**
4.1 Methods of Simulation 8
4.2 Description of the Three Orbits Studied 9
4.3 Orbit I 9
4.4 Orbit II 11
4.5 Orbit III 13

5 Conclusions **15**

List of Figures

3.1.1 Double spherical pendulum 6
4.3.1 Trace of the two masses for orbit I: (a) inertial frame (b) critical angular velocity. Projection of the traces: (c) inertial frame (d) critical angular velocity 10
4.3.2 Resonant patterns for orbit I (a) $\gamma = 0.4705$ (b) $\gamma = 0.8550$ (c) $\gamma = 1.0430$ (d) $\gamma = 2.7580$ 11
4.4.1 Trace of the two masses for orbit II: (a) inertial frame (b) critical angular velocity. Projection of the traces: (c) inertial frame (d) critical angular velocity 12
4.4.2 Resonant patterns for orbit II (a) $\gamma = 0.4220$ (b) $\gamma = 0.6250$ (c) $\gamma = 2.0840$ (d) $\gamma = 2.5000$ 13
4.5.1 Trace of the two masses for Orbit III: (a) inertial frame (b) critical angular velocity. Projection of the traces: (c) inertial frame (d) critical angular velocity 14
4.5.2 Resonant patterns for orbit III (a) $\gamma = 0.2520$ (b) $\gamma = 0.8645$ (c) $\gamma = 2.0880$ (d) $\gamma = 3.3110$ 15
4.5.3 Resonant Pattern for orbit III, $\gamma = 0.8645$ 16

1 Introduction

This paper is an exploration of pattern evocation in the double spherical pendulum (DSP). Patterns have been discovered in mechanical systems when the orbits of the system are viewed in a rotating frame. This phenomena was observed for point vortices in Kunin, Hussain, Zhou, and Prishepionok [1992]. Marsden and Scheurle [1995] have developed a theory for this phenomenon.

In the present paper we summarize the theory and illustrate it with a numerical study of the double spherical pendulum. The numerical simulations are done using the differential algebraic multibody system solver called MEXX and an energy-momentum integrator as a check. However, the numerical aspects of these integrators as well as a comparison of their performance is not discussed here.

2 Summary of the Theory on Pattern Evocation

This section provides a summary of some of the theory in Marsden and Scheurle [1995]. A result of this paper is that if there is a periodic (respectively, quasiperiodic or almost periodic) orbit in the reduced space, then when viewed in a suitably chosen rotating frame with *constant* angular velocity, the motion in the unreduced space is also periodic (respectively, quasiperiodic or almost periodic). The role of discrete symmetries in visualizing orbits is also discussed.

2.1 Uniform Frames for Equivariant Dynamical Systems

The general context is as follows. Let G be a Lie group acting on a manifold M and let X be a vector field that is $G-$invariant. The flow of X produces a one parameter group of equivariant transformations, $F_t : M \to M$, which induces a reduced flow, $\phi_t : M/G \to M/G$ on the orbit space, M/G. In this case, $\pi \circ F_t = \phi_t \circ \pi$, where $\pi : M \to M/G$ is the projection of the manifold to the orbit space. A fixed point, $s \in M/G$, corresponds to a relative equilibrium orbit in $\pi^{-1}(s)$. If there is a periodic orbit in the reduced space, the corresponding motion in the unreduced space is called a *relative periodic orbit*. A relative equilibrium through a point $z_0 \in M$ is given by

$$z(t) = \exp(t\gamma) z_0$$

for some $\gamma \in \mathfrak{g}$, the Lie algebra of G. Viewing the motion of the relative equilibrium in a moving frame with constant velocity γ means that we replace $z(t)$ by $\exp(-\gamma t)z(t)$. In this frame, the motion appears to be fixed.

One introduces the term "relatively quasiperiodic orbit" in a similar way.

The following theorem generalizes the above observation about relative equilibria to the case of relatively periodic orbits:

Theorem 2.1 *Assume that the exponential map* $\exp : \mathfrak{g} \to G$ *is surjective. Assume that* $c(t)$ *is a relative periodic orbit and denote a period of the reduced orbit by* T*. Then there is a Lie algebra element* $\gamma \in \mathfrak{g}$ *such that* $\exp(-\gamma t)c(t)$ *is also periodic with period* T*.*

2.2 Symplectic Reduction

Symplectic reduction gives one context in which one can apply this theorem. Let P be a symplectic manifold and G a Lie group acting on P. Let $\mathbf{J} : P \to \mathfrak{g}^*$ be an Ad^*-equivariant momentum map. For a fixed value μ of $\mathbf{J}$, let $G_\mu = \{g \in G \mid \mathrm{Ad}^*_{g^{-1}} \cdot \mu = \mu\}$ be the isotropy subgroup of G with Lie algebra $\mathfrak{g}_\mu$. The symplectic reduced space is $P_\mu = \mathbf{J}^{-1}(\mu)/G_\mu$. Given a G-invariant Hamiltonian H on P we get a corresponding G-invariant vector field X_H on P and the associated dynamics.

Theorem 2.2 *Assume that the exponential map* $\exp : \mathfrak{g}_\mu \to G_\mu$ *is surjective. Assume that* $c(t)$ *is a relative periodic orbit and denote the period of the flow in the reduced orbit by* T*. Then there is a Lie algebra element* $\gamma \in \mathfrak{g}_\mu$ *such that* $\exp(-\gamma t)c(t)$ *is also periodic with period* T*.*

2.3 Cyclic Coordinates and the Frame Angular Velocity Formula

More detailed information about the nature of these rotating frames is provided by studying Lagrangian systems with cyclic coordinates. We consider Lagrangians, $L(x, \dot{x}, \dot{\theta})$, where $x = (x^1, \ldots, x^m)$ are internal variables and where $\theta = (\theta^1, \ldots, \theta^k)$ are cyclic coordinates of the following form:

$$L(x, \dot{x}, \dot{\theta}) = \frac{1}{2} g_{\alpha\beta} \dot{x}^\alpha \dot{x}^\beta + g_{a\beta} \dot{\theta}^a \dot{x}^\beta + \frac{1}{2} g_{ab} \dot{\theta}^a \dot{\theta}^b - V(x). \tag{2.3.1}$$

Here, the total kinetic energy defines the Riemannian metric g (the mass matrix) which has components in the x and the θ variables, as well as cross terms, and $V(x)$ is the potential energy. The locked inertia tensor, $\mathbb{I} : \mathfrak{g} \to \mathfrak{g}^*$, has components given by $\mathbb{I}_{ab} = g_{ab}$ in this case; see for example, Marsden [1992] for the definition in a more general context. When one does reduction, the cyclic variables are eliminated and so one views reduced trajectories in the velocity phase space of the x's.

Theorem 2.3 *Suppose that* $q(t) = (x(t), \theta(t))$ *is a solution of the Euler-Lagrange equations on* Q *and that the reduced trajectory* $x(t)$ *is periodic with period* T*. Then relative to the frame with angular velocity given by*

$$\gamma^a = \frac{1}{T} \int_0^T \mathbb{I}^{ca}(x(t)) \mu_c dt - \frac{1}{T} \int_0^T g_{\alpha c}(x(t)) \dot{x}^\alpha(t) \mathbb{I}^{ca}(x(t)) dt, \tag{2.3.2}$$

the solution $q(t)$ *is also periodic with period* T*.*

The values of γ determined by this formula correspond to what we later call the critical angular velocities for the double spherical pendulum.

2.4 Quasiperiodic Orbits

A function, $x(t)$, is *quasiperiodic* if $x(t) = \phi(\omega_1 t, \omega_2 t, ..., \omega_n t)$ for some function ϕ that is 2π periodic in all of its arguments and for some finite number of frequencies, ω_1 to ω_n. The following theorem relates quasiperiodic motion in the reduced space to a suitably transformed motion in unreduced space.

Theorem 2.4 *Suppose that* $q(t)$ *is a solution of the Euler-Lagrange equations on* Q *and that the reduced trajectory is quasiperiodic with the frequencies* $\omega_1, ..., \omega_n$ *such that the following nonresonance condition is satisfied:*

$$\left| \sum_{k=1}^n j_k \omega_k \right| \geq \rho \|j\|^{-\tau}, \tag{2.4.1}$$

where ρ *and* τ *are certain positive constants and the norm is any convenient one on* n*-space. Assume that the kinetic and potential energy functions are* C^k *for* $k \geq \tau + 2$*. Then, relative to a frame with the angular velocity given by the formula*

$$\gamma^a = \lim_{T \to \infty} \frac{1}{T} \int_0^T \left[\mathbb{I}^{ca}(x(t)) \mu_c - g_{\alpha c}(x(t)) \dot{x}^\alpha(t) \mathbb{I}^{ca}(x(t)) \right] dt, \tag{2.4.2}$$

the solution $q(t)$ *is also quasiperiodic with the frequencies* $\omega_1, ..., \omega_n$*.*

A similar result holds for almost periodic functions. A function, $f(t)$, is *almost periodic* if given any $\epsilon > 0$, there is a positive real number $T = T(\epsilon)$ such that any interval of length T on the real axis contains a number τ with $|f(t + \tau) - f(t)| \leq \epsilon$ for all $t \in \mathbb{R}$.

2.5 Discrete Symmetries

Discrete symmetries may exist in a particular problem and may induce discrete symmetries in the reduced space. We now discuss how a discrete symmetry of a trajectory in the reduced space is visualized in the original space.

Let (P,Ω) be a symplectic manifold with a Lie group G acting on P. Let $\mathbf{J} : P \to \mathfrak{g}^*$ be an Ad*-equivariant momentum map for the action of G. The discrete group is denoted by Σ. We assume that Σ acts on G by group homomorphisms and denote the action of an element $\sigma \in \Sigma$ by $\sigma_G : G \to G$. We also assume that Σ acts on P by symplectic or antisymplectic transformations and denote the action of σ by $\sigma_P : P \to P$. Antisymplectic transformations change the sign of the symplectic form. Σ has a subgroup Σ_s consisting of the symplectic transformations. The subset of antisymplectic transformations is denoted $\Sigma_a \subset \Sigma$. Let $\sigma_{\mathfrak{g}} : \mathfrak{g} \to \mathfrak{g}$ be the Lie algebra homomorphism obtained by taking the derivative of σ_G at the identity. Let $\sigma_{\mathfrak{g}^*} : \mathfrak{g}^* \to \mathfrak{g}^*$ be the dual of $(\sigma^{-1})_{\mathfrak{g}}$.

We make several assumptions that guarantee that the discrete symmetries have a well defined action on the symplectic reduced space.

Assumption 1 *The actions of G and Σ are compatible in the sense that the following equation holds:*

$$\sigma_P \circ g_P = [\sigma_G(g)]_P \circ \sigma_P. \tag{2.5.1}$$

This assumption implies that Σ has a well defined action on P/G.

A simple example that is useful in the double spherical pendulum is as follows. Let $G = SO(2)$ regarded as the group of rotations in space around the z-axis and let Σ be the group of reflections in a chosen vertical plane, such as the xz-plane. We choose $\sigma_G(g)$ to be conjugation, *i.e.*, $\sigma g \sigma^{-1} \in G$.

Differentiating equation 2.5.1 in the direction of $\gamma \in \mathfrak{g}$ results in

$$\mathbf{J} \circ \sigma_P = \pm \sigma_{\mathfrak{g}^*} \circ \mathbf{J} + (\text{cocycle}). \tag{2.5.2}$$

The paper assumes that the cocycle is zero and this leads to the following assumption.

Assumption 2 *The following equation holds:*

$$\mathbf{J} \circ \sigma_P = \pm \sigma_{\mathfrak{g}^*} \circ \mathbf{J} \tag{2.5.3}$$

where the plus sign is used for $\sigma \in \Sigma_s$ and the minus sign is used for $\sigma \in \Sigma_a$.

These assumptions as well as the additional assumption that σ_P preserves the momentum map implies that Σ has a well defined action on the symplectic reduced space.

Let $w(t) \in P/G$ be a time dependent orbit and assume that it has the discrete symmetry $(\sigma_0, l_0) \in \Sigma \times \mathbb{R}$, where $\mathbb{R}$ acts by time shifts, *i.e.*,

$$\sigma_0 w(\pm(t - l_0)) = w(t) \tag{2.5.4}$$

for all time. The plus sign corresponds to symplectic transformations and the minus sign corresponds to antisymplectic transformations. Let $c(t)$ be an orbit that projects to $w(t)$ and let

$$\tilde{c}(t) = \exp(-\gamma t) c(t) \tag{2.5.5}$$

be the transformed data in a rotating frame with velocity γ. It is shown in Marsden and Scheurle [1995] that

$$\sigma_0 \tilde{c}(\pm(t - l_0)) = g_0 \tilde{c}(t) \tag{2.5.6}$$

holds for some $g_0 \in G$ and for all $t \in \mathbb{R}$ provided that the momentum map, $\mathbf{J}$, is σ_0-invariant. We then seek a $g_1 \in G$ such that

$$\sigma_0 g_1 \tilde{c}(\pm(t - l_0)) = g_1 \tilde{c}(t), \tag{2.5.7}$$

or equivalently,

$$g_1^{-1}\sigma_0 g_1 \tilde{c}(\pm(t-l_0)) = \tilde{c}(t). \tag{2.5.8}$$

This last equation shows that $\tilde{c}(t)$ has the discrete symmetry $(g_1^{-1}\sigma_0 g_1, l_0)$. If $G = SO(2)$ and Σ is the group of reflections in a vertical plane, then $g_1^{-1}\sigma_0 g_1$ is a reflection in a plane rotated by g_1^{-1}.

Using equation 2.5.6 and equation 2.5.8, it can be shown that such a g_1 exists if there is a g_1 that solves the following equation:

$$\sigma_0 g_1^{-1}\sigma_0^{-1} g_1 = g_0. \tag{2.5.9}$$

In the case where $G = SO(2)$ and Σ is the group of reflections in vertical planes, one can take g_1 to be the square root of g_0 (a rotation through half the angle).

3 The Double Spherical Pendulum System

We now explain how the double spherical pendulum (DSP) fits into the above context.

3.1 The Configuration Space, Lagrangian and Hamiltonian

The double spherical pendulum system is shown in figure 3.1.1.

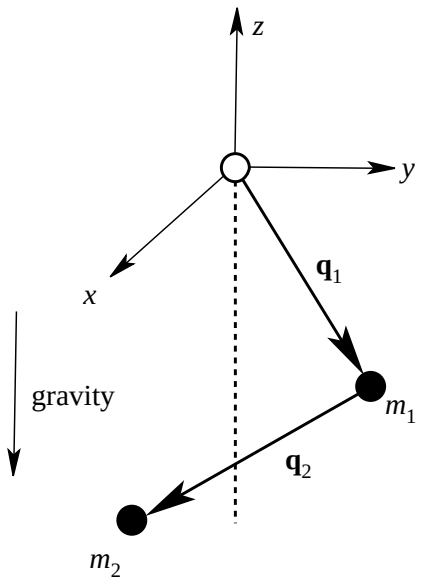

Figure 3.1.1: Double spherical pendulum

We let the position vectors of each pendulum relative to their hinge points be denoted $\mathbf{q}_1$ and $\mathbf{q}_2$. These vectors are assumed to have fixed lengths l_1 and l_2 and the pendula masses are denoted m_1 and m_2. The configuration space is $Q = S^2_{l_1} \times S^2_{l_2}$, the product of spheres of radii l_1 and l_2, respectively. The Lagrangian is

$$L(\mathbf{q}_1, \mathbf{q}_2, \dot{\mathbf{q}}_1, \dot{\mathbf{q}}_2) = \frac{1}{2}m_1\|\dot{\mathbf{q}}_1\|^2 + \frac{1}{2}m_2\|\dot{\mathbf{q}}_1 + \dot{\mathbf{q}}_2\|^2 - m_1 g\mathbf{q}_1 \cdot \mathbf{k} - m_2 g(\mathbf{q}_1 + \mathbf{q}_2) \cdot \mathbf{k}, \tag{3.1.1}$$

where $\mathbf{k}$ is the unit vector along the z-axis. Since $\mathbf{q}_1 + \mathbf{q}_2$ represents the position of the second mass relative to an inertial frame, (3.1.1) has the standard form of kinetic minus potential energy. We identify the velocity vectors $\dot{\mathbf{q}}_1$ and $\dot{\mathbf{q}}_2$ with vectors perpendicular to $\mathbf{q}_1$ and $\mathbf{q}_2$, respectively.

The conjugate momenta are

$$\mathbf{p}_1 = \frac{\partial L}{\partial \dot{\mathbf{q}}_1} = m_1\dot{\mathbf{q}}_1 + m_2(\dot{\mathbf{q}}_1 + \dot{\mathbf{q}}_2) \tag{3.1.2}$$

and

$$\mathbf{p}_2 = \frac{\partial L}{\partial \dot{\mathbf{q}}_2} = \mathbf{m}_2(\dot{\mathbf{q}}_1 + \dot{\mathbf{q}}_2) \tag{3.1.3}$$

regarded as vectors in $\mathbb{R}^3$ that are only paired with vectors orthogonal to $\mathbf{q}_1$ and $\mathbf{q}_2$ respectively.

The Hamiltonian is therefore

$$H(\mathbf{q}_1, \mathbf{q}_2, \mathbf{p}_1, \mathbf{p}_2) = \frac{1}{2m_1}\|\mathbf{p}_1 - \mathbf{p}_2\|^2 + \frac{1}{2m_2}\|\mathbf{p}_2\|^2 + m_1 g\mathbf{q}_1 \cdot \mathbf{k} + m_2 g(\mathbf{q}_1 + \mathbf{q}_2) \cdot \mathbf{k}. \tag{3.1.4}$$

The equations of motion are given by the Euler-Lagrange equations for L on TQ or, equivalently by Hamilton's equations for H on T^*Q. For the explicit form of these equations and further results, see Marsden and Scheurle [1993a,b].

3.2 Symmetries

The continuous symmetry group of the DSP is the group of rotations about the z-axis and the corresponding conserved quantity (the momentum map) is the standard angular momentum about the z-axis.

In addition to this continuous symmetry group, the double spherical pendulum (DSP) has two discrete symmetries: a reflection symmetry in a vertical plane and a time reversal symmetry. Time reversal sends $t \mapsto -t$, $q_i \mapsto q_i$, and $\dot{q}_i \mapsto -\dot{q}_i$. The reflection symmetry is a symplectic transformation while the time reversal symmetry is an antisymplectic transformation. Both transformations change the sign of the momentum map so they do not separately provide a well defined action on the symplectic reduced space. If the actions of reversals and reflections are composed (the order does not matter since they commute), then the momentum map is preserved and this combination of the discrete groups has a well defined action on the reduced space.

3.3 The Reduced Variables

The reduced variables are obtained by setting the angular momentum equal to a constant and taking the quotient space with the continuous symmetry group S^1. The resulting phase space is that associated with the configuration space quotient, Q/G. Convenient coordinates for this reduced configuration space (with the straight down state removed) are r_1, r_2, θ where r_i is the radial component of the projection of the position vector of the ith bob onto the horizontal plane and θ is the angle between two vertical planes, each of which contains one of the bobs and the z-axis. In the general theory earlier, the x coordinates are (r_1, r_2, θ) and the cyclic coordinate is, for example, the angle of the first bob relative to the xz plane, taken in the inertial frame.

4 Simulation Results and Patterns

4.1 Methods of Simulation

A differential algebraic equation (DAE) model of the double spherical pendulum (DSP) is obtained and integrated by MEXX, a multibody simulation package developed by Lubrich, Nowak, Pöhle, and Engstler [1992]. The DAE model enforces the length constraints in the DSP through Lagrange multipliers. An energy-momentum integrator was also created to integrate the equations of motion following the ideas of Gonzales and Simo [1994], Simo and Gonzales [1993], Simo and Tarnow [1992] and Tarnow [1993]. See Wendlandt [1995] for a description of the energy-momentum algorithm for the DSP. This integrator has the property that it exactly preserves the energy and angular momentum; it deals with the constraints in a similar way as the DAE method in that an implicit equation is solved to enforce the constraints as the algorithm proceeds. The MEXX simulation leads to systematic energy and angular momentum errors, but the computations below are shown only for times during which both methods give solutions that differ by a small amount. We should also point out that a symplectic-momentum integrator for the DSP was developed and studied by McLaughlin and Scovel [1995].

MEXX integrates nonstiff equations of motion for mechanical systems in the following form:

$$\begin{aligned} \dot{p} &= T(t,p)v && (4.1.1)\\ M(t,p)\dot{v} &= f(t,p,v,\lambda,u) - G(t,p)^T\lambda && (4.1.2)\\ 0 &= G(t,p)\cdot v + g^I(t,p) && (4.1.3)\\ \dot{u} &= d(t,p,v,\lambda,u), && (4.1.4) \end{aligned}$$

where $p(t)$ are the position variables, $v(t)$ are the velocity variables, $\lambda(t)$ are the Lagrange multipliers, and $u(t)$ are optional external dynamics. The position constraints are

$$0 = g(t,p). \tag{4.1.5}$$

The velocity constraints are contained in equation 4.1.3. The user specifies the initial conditions for the simulation, namely $p(t_0), v(t_0)$, and $u(t_0)$. External dynamics can include control inputs but are not used in the DSP model. The DSP equations on the full configuration space described in the previous section are readily cast into this form.

In applying these methods, Matlab and Mathematica scripts are used to display the data and transform the data to rotating frames. The velocity of the rotating frame is varied until a pattern appears (we call these *resonant angular velocities*) or until the critical velocity is determined. The critical velocity in the simulations are distinguished by the fact that relative to these frames the bobs do not encircle the z-axis. As we said earlier, this value is determined by the frame angular velocity formula (2.3.2).

The position coordinates of each bob in the inertial frame are transformed to position coordinates in a frame with angular velocity vector ω_γ, the vector along the z-axis with length γ, by the equation

$$\begin{bmatrix} \tilde{q}_1(t) \\ \tilde{q}_2(t) \end{bmatrix} = e^{-\hat{\omega}_\gamma t} \begin{bmatrix} I & 0 \\ 0 & I \end{bmatrix} \begin{bmatrix} q_1(t) \\ q_2(t) \end{bmatrix}, \tag{4.1.6}$$

where

$$\hat{\omega}_\gamma = \begin{bmatrix} 0 & -\gamma & 0 \\ \gamma & 0 & 0 \\ 0 & 0 & 0 \end{bmatrix}. \tag{4.1.7}$$

The new position data, $(\tilde{q}_1(t), \tilde{q}_2(t))$, is then graphed and reveals patterns for particular angular velocities and for particular initial conditions. The transformed data is the data as viewed in a camera looking down the z-axis that is rotating with angular velocity γ.

4.2 Description of the Three Orbits Studied

Several cases of pattern evocation in the DSP are shown below. Each case corresponds to a different set of initial conditions so that each case corresponds to the study of a particular orbit.

The first orbit is close to a relative equilibrium of the double spherical pendulum system, namely one in which the two bobs are nearly aligned. (Another class of relative equilibria for the system are the *cowboy* solutions). This orbit does not appear to have a periodic motion in the reduced space but still reveals patterns for particular camera angular velocities. In the critical angular velocity frame, the orbit seems to have structure in that, for example, the lower bob moves on a trajectory that is reasonably close to elliptical in shape.

The second orbit is one in which the bobs are more nearly in the straight down state. In this case, the motion in the critical frame also has structure and patterns are again observed. The orbit in the reduced space again appears to be not periodic.

The third orbit is one in which the motion in the critical frame is less structured. In fact, in this case, we deliberately looked for a more complex orbit.

For each simulation, the trace of the two masses in an inertial frame is shown as well as the motion in the frame with critical angular velocity. The projections of the orbits onto a horizontal plane are also shown; in view of the length constraints, one looses no information by this projection. The patterns that one sees relative to various rotating frames are shown as well.

In the following simulations, the data and units that are used are $m_1 = 2.0\text{kg}$, $m_2 = 3.5\text{kg}$, $l_1 = 4.0\text{m}$, $l_2 = 3.0\text{m}$, and $g = 9.81\text{m/s}^2$.

4.3 Orbit I

The initial conditions for the first orbit are $x_1 = 2.820\text{m}$, $y_1 = 0.025\text{m}$, $x_2 = 5.085\text{m}$, $y_2 = 0.105\text{m}$, $\dot{x}_1 = 3.381\text{m/s}$, $\dot{y}_1 = 2.506\text{m/s}$, $\dot{x}_2 = 2.497\text{m/s}$, and $\dot{y}_2 = 10.495\text{m/s}$. The position and velocity of the z-coordinate is determined from the constraints and the z-coordinate for both masses is taken to be negative. This motion is close to a relative equilibrium. The initial conditions for the relative equilibrium are $x_1 = 3.0788\text{m}$, $y_1 = 0.0\text{m}$, $x_2 = 5.5418\text{m}$, $y_2 = 0.0\text{m}$, $\dot{x}_1 = 0.0\text{m/s}$, $\dot{y}_1 = 4.8593\text{m/s}$, $\dot{x}_2 = 0.0\text{m/s}$, and $\dot{y}_2 = 8.7468\text{m/s}$.

The trajectory of the two masses in an inertial frame and their projections onto the horizontal plane is shown in figure 4.3.1(a). This motion projected onto the xy plane is shown again in figure 4.3.1(c). The motion in the frame with the critical angular velocity is shown in figure 4.3.1(b) and 4.3.1(d). With the critical velocity, the motion of the outer mass appears to move in an approximately elliptical orbit while the inner mass moves in what appears to be an orbit with more than one frequency.

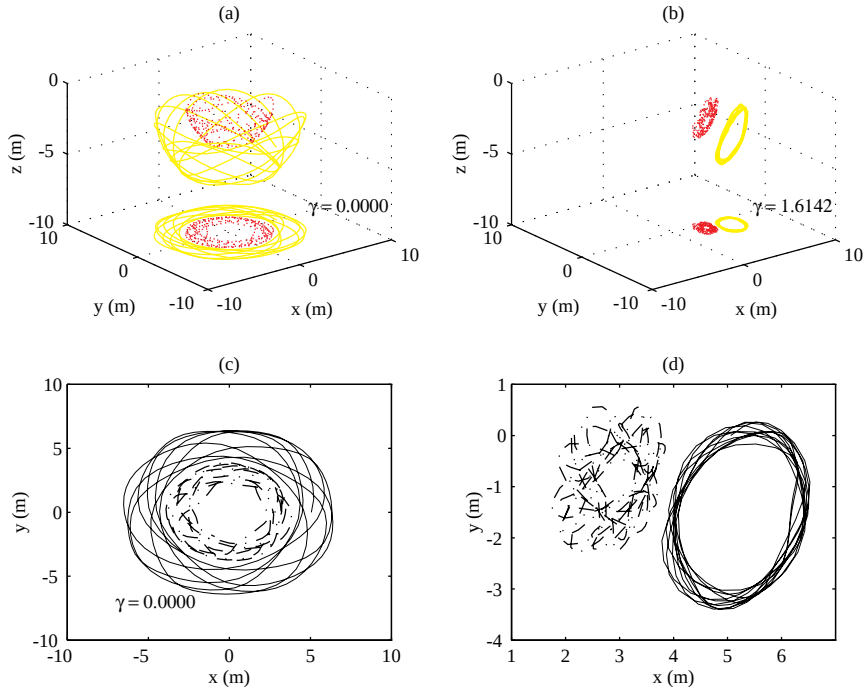

Figure 4.3.1: Trace of the two masses for orbit I: (a) inertial frame (b) critical angular velocity. Projection of the traces: (c) inertial frame (d) critical angular velocity

Four resonant patterns are shown in figure 4.3.2. The angular velocity of the frame is below the critical angular velocity in figure 4.3.2(a)-(c) and above the critical angular velocity for figure 4.3.2(d). The pattern in figure 4.3.2(a) has an approximately elliptical shape in the outer mass and a less well approximated ellipse for the inner mass. A trajectory resembling a triangle appears in the next pattern. This pattern has the discrete symmetries of D_3, the symmetry group of an equilateral triangle. A trajectory having (approximately) the symmetry group D_4 of a square is revealed in the next pattern. The last resonant pattern clearly has (an approximate) D_2 symmetry.

There is an interesting relationship between the angular velocities that evoke a pattern, the critical angular velocity, and the discrete symmetry observed. Let γ_c be the critical angular velocity and γ_n be the angular velocity associated with an n-fold symmetry. Assuming the reduced orbit is periodic, let F be its period. Then

$$|\gamma_c - \gamma_n| = \frac{m}{n} F, \tag{4.3.1}$$

where m and n are positive integers. This equation is seen by exploiting the resonance between the frequency of the camera motion and the frequency of the reduced orbit.

If the reduced orbit has a reflection symmetry, then the patterns are not only n-fold symmetric, but have reflection symmetries as well; that is, they are D_n-symmetric. This is the case for the orbits we examined and is consistent with the discrete symmetry theory described earlier. In other words, the patterns can be explained by the resonance between the camera and the reduced orbit together with the reflection symmetry of the reduced orbit.

We now explore equation (4.3.1) for the resonant patterns even though the reduced orbit does not appear to be periodic. A D_4 symmetric orbit is shown in figure 4.3.2(c) and the corresponding angular velocity is $\gamma_4 = 1.0403$ (given in radians per second). The critical angular velocity is

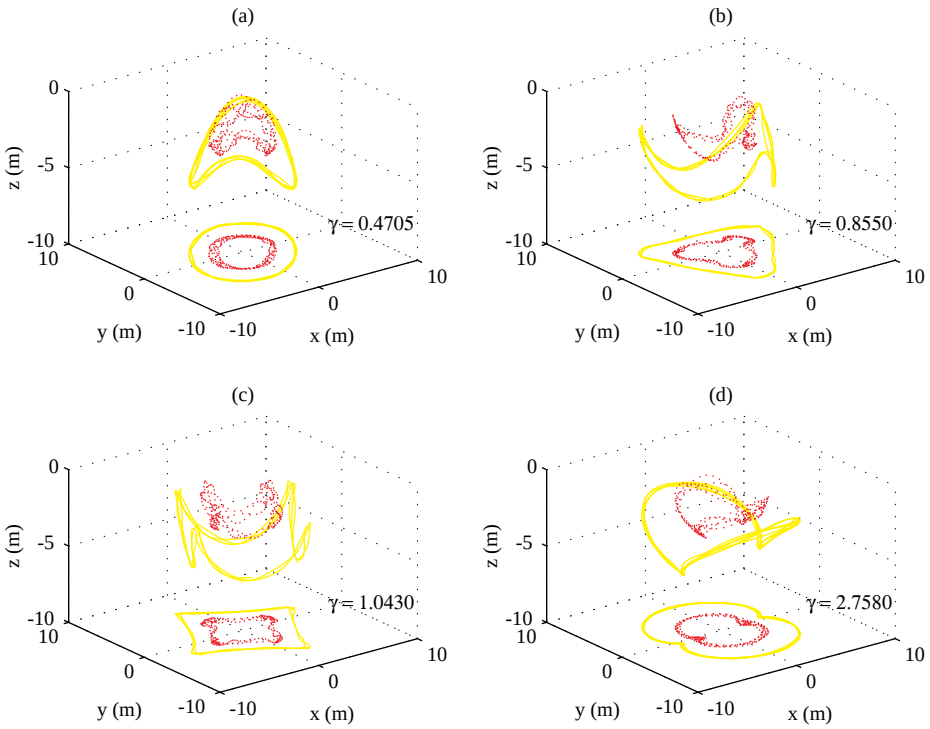

Figure 4.3.2: Resonant patterns for orbit I (a) $\gamma = 0.4705$ (b) $\gamma = 0.8550$ (c) $\gamma = 1.0430$ (d) $\gamma = 2.7580$

$\gamma_c = 1.6142$. Using equation 4.3.1, F is found to be 2.2848s. For the pattern in figure 4.3.2(b), $\gamma_3 = 0.8550$ and equation 4.3.1 predicts that F (given in seconds) is 2.2776s. The patterns in figure 4.3.2(a) and 4.3.2(d) both have a D_2 symmetry group. For the pattern shown in figure 4.3.2(a), the predicted value for F is 2.2874s, and for figure 4.3.2(d), F is predicted to be 2.2876s. The largest difference between the calculated F's is 0.01. Thus, in this case, the relation (4.3.1) holds rather well.

We remark that this orbit plotted in the reduced position coordinates r_1, r_2, θ (we do not reproduce it here) appears to have less structure than the orbits in figure 4.3.1(b).

It is helpful to watch a movie of the transformed position trajectories parameterized by the angular velocity. Such a movie for orbit I may be seen at http://avalon.caltech.edu:80/cds/cgi-bin/reports.cgi (search for the report with the title *Visualization of orbits and pattern evocation for the double spherical pendulum*).

4.4 Orbit II

The initial conditions for this simulation resulted from varying the initial conditions of the two masses hanging straight down and at rest. The initial conditions are $x_1 = 0.012$m, $y_1 = 0.009$m, $x_2 = 0.505$m, $y_2 = 0.510$m, $\dot{x}_1 = 0.210$m/s, $\dot{y}_1 = -0.040$m/s, $\dot{x}_2 = -0.477$m/s, and $\dot{y}_2 = 0.023$m/s.

In figure 4.4.1, the motion in the inertial frame and the frame with the critical angular velocity are shown. The motion in the critical frame shows the outer mass moving in a circular motion and the inner mass moving in a trajectory resembling a "figure eight". The critical angular velocity is $\gamma_c = 1.253$.

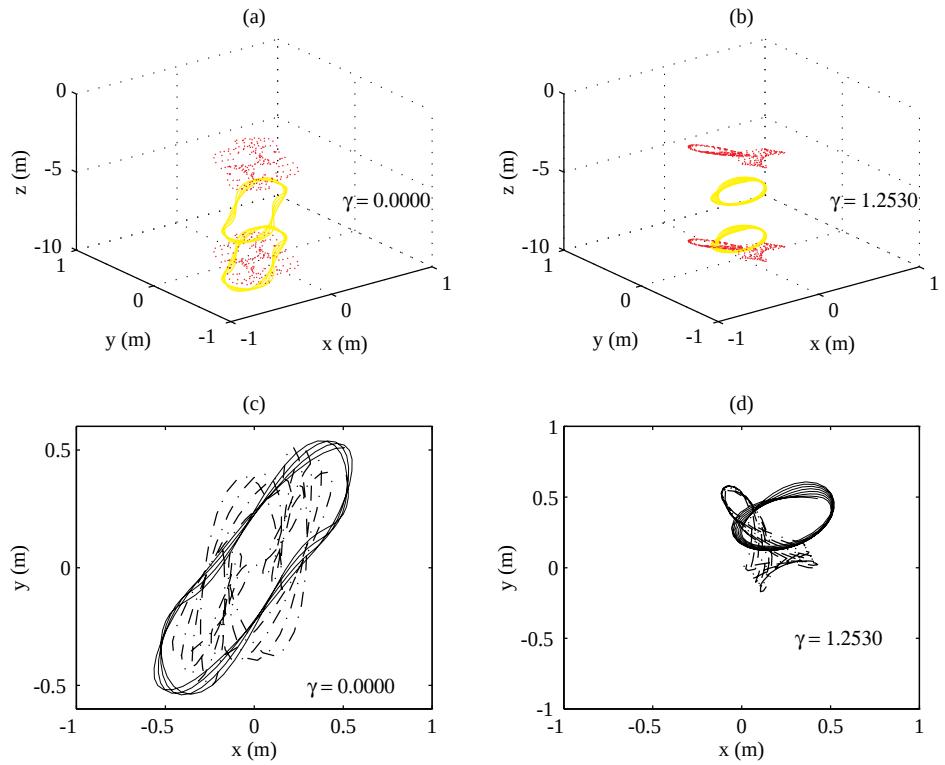

Figure 4.4.1: Trace of the two masses for orbit II: (a) inertial frame (b) critical angular velocity. Projection of the traces: (c) inertial frame (d) critical angular velocity

Figure 4.4.2 reveals four resonant patterns. Figure 4.4.2(a) and 4.4.2(b) result from angular velocities below γ_c and 4.4.2(c) and 4.4.2(d) result from angular velocities above γ_c. The pattern in figure 4.4.2(a) and 4.4.2(c) have a D_3 symmetry. Figure 4.4.2(b) has a D_4 symmetry and figure 4.4.2(d) has a D_2 symmetry.

The numerology formula (4.3.1) seems to apply to this example as well. For the resonant pattern shown in figure 4.4.2(a), the value of F calculated from equation 4.3.1 is 2.493. F is 2.512 for figure 4.4.2(b), F is 2.493 for figure 4.4.2(c), and F is 2.494 for figure 4.4.2(d). The largest difference in the calculated F's is 0.019.

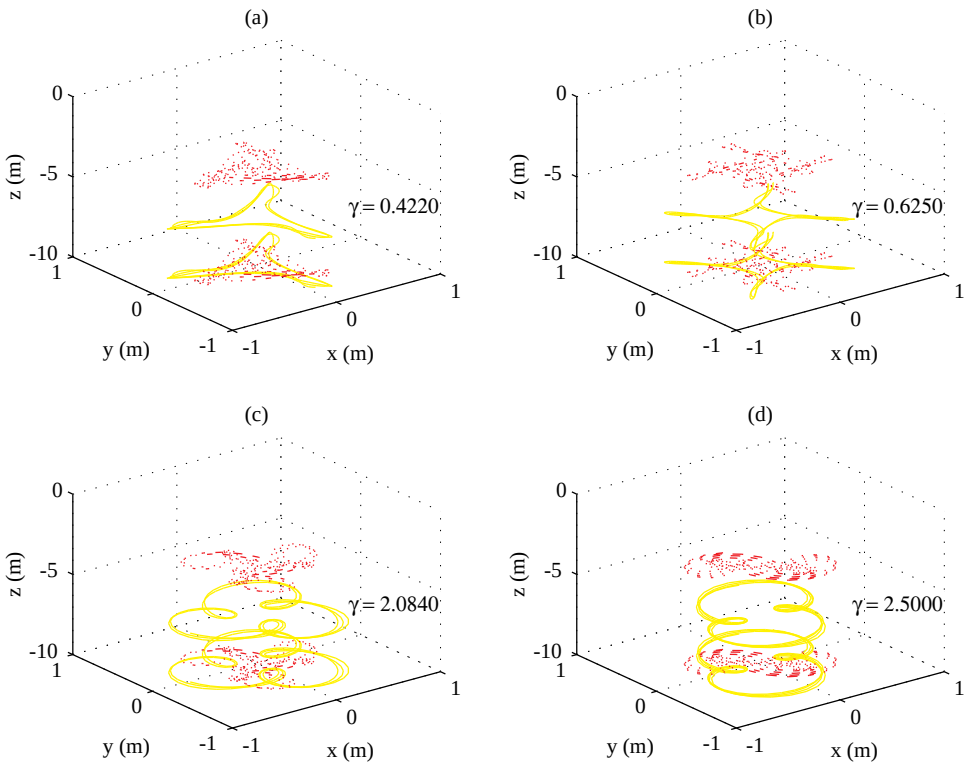

Figure 4.4.2: Resonant patterns for orbit II (a) $\gamma = 0.4220$ (b) $\gamma = 0.6250$ (c) $\gamma = 2.0840$ (d) $\gamma = 2.5000$

4.5 Orbit III

The initial conditions for this simulation are $x_1 = 4.000\text{m}$, $y_1 = 0.000\text{m}$, $x_2 = 4.000\text{m}$, $y_2 = 0.060\text{m}$, $\dot{x}_1 = -0.001\text{m/s}$, $\dot{y}_1 = 0.001\text{m/s}$, $\dot{x}_2 = 0.000\text{m/s}$, and $\dot{y}_2 = 6.000\text{m/s}$.

The motion in the inertial frame is shown in figure 4.5.1(a) and 4.5.1(c). The motion as seen from the frame with the critical angular velocity, $\gamma_c = 1.4803$, is shown in figure 4.5.1(b) and 4.5.1(d). The motion in figure 4.5.1(d) resembles a set with a reflection symmetry about the x-axis.

Four resonant patterns are shown in figure 4.5.2. A D_2 symmetry is revealed in each of the patterns, which is the same discrete symmetry that is posessed by the orbit in the frame with critical angular velocity.

Equation (4.3.1) predicts values of F with surprizing consistency for this example as well. The period F is calculated to be 1.2283 for $\gamma_2 = 0.2520$ with $m = 2$, 1.2316 for $\gamma_2 = 0.8645$ with $m = 1$, 1.2154 for $\gamma_2 = 2.0880$ with $m = 1$, and 1.2205 for $\gamma_2 = 3.3110$ with $m = 3$. The calculated values of F vary from 1.2154 to 1.2316 with the average being 1.2240.

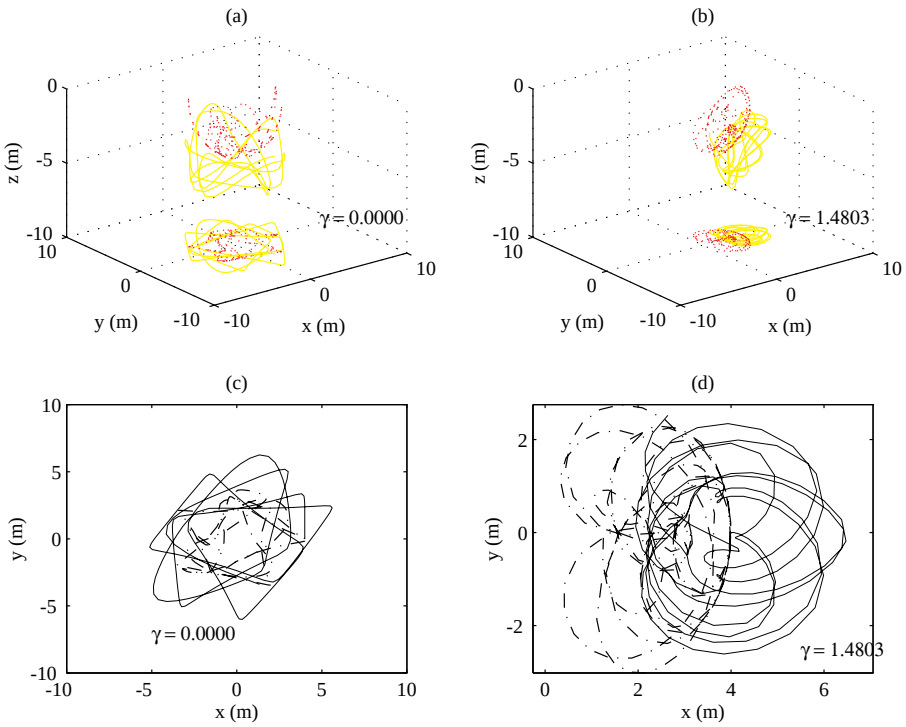

Figure 4.5.1: Trace of the two masses for Orbit III: (a) inertial frame (b) critical angular velocity. Projection of the traces: (c) inertial frame (d) critical angular velocity

In each of the four patterns shown in figure 4.5.2, the pattern seems to dissappear after further integration, even with numerical errors in control. However, these patterns could be reinstated upon even longer integration, but this would require more careful integrations than we have attempted. The loss of the pattern is illustrated in figure 4.5.3 for $\gamma_2 = 0.8645$. The initial position is at $(x_2, y_2) = (4, 0)$ and the position of the second mass at $t = 20s$ is labeled in the figure.

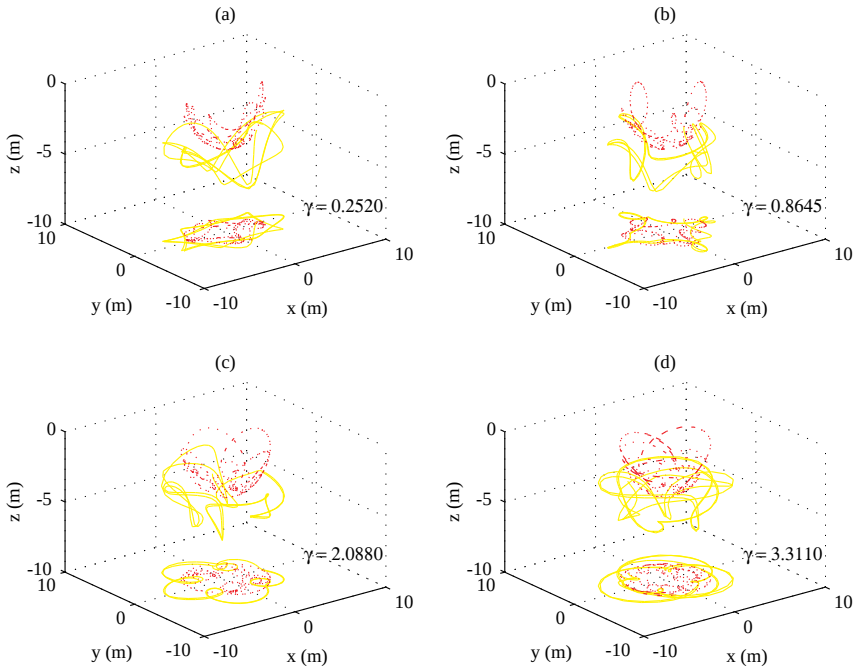

Figure 4.5.2: Resonant patterns for orbit III (a) $\gamma = 0.2520$ (b) $\gamma = 0.8645$ (c) $\gamma = 2.0880$ (d) $\gamma = 3.3110$

5 Conclusions

This paper began by presenting the background on the theory of pattern evocation given by Marsden and Scheurle [1995]. The theory demonstrates an interaction between continuous groups, reduced phase spaces, the geometric phase and discrete symmetries in the evocation of patterns. Several numerical examples presented in this paper of pattern evocation in the double spherical pendulum show a fairly good agreement with the theory. Of course we are not sure to what extent the precise hypotheses of the theory (especially the delicate number theoretic conditions on the frequencies of quasiperiodic motions) are really satisfied; nonetheless, there is good agreement with the main conclusions of that theory. In the future it would be of interest to make connections with works on the symmetry structure of invariant sets and attractors, for example, Melbourne, Dellnitz, and Golubitsky [1993].

Acknowledgments

We thank Michael Dellnitz, Marty Golubitsky, Isaac Kunin, Sergy Prishepionok, and Ian Melbourne for useful comments.

References

Gonzales, O. and J.C. Simo [1994] On the stability of Symplectic and Energy-Momentum Algorithms for Nonlinear Hamiltonian Systems with Symmetry. *preprint.*

Kunin, I., F. Hussain, X. Zhou, and S.J. Prishepionok [1992]. Centroidal frames in dynamical systems I. Point vortices, *Proc. Roy. Soc. Lon. A* **439**, 441–463.

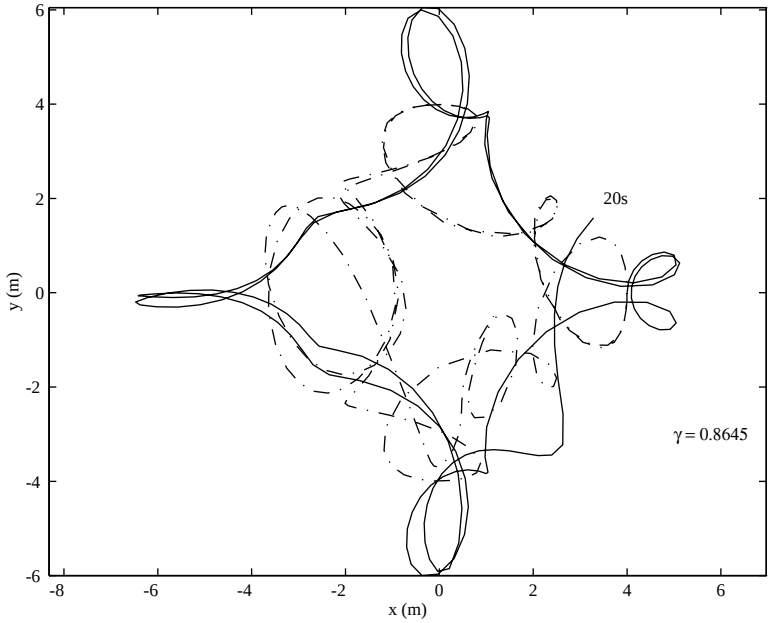

Figure 4.5.3: Resonant Pattern for orbit III, $\gamma = 0.8645$

Lubrich, Ch, U. Nowak, U. Pöhle and Ch. Engstler [1992] MEXX - Numerical Software for the Integration of Constrained Mechanical Multibody Systems. *Konrad-Zuse-Zentrum für Informationstechnik Berlin (ZIB)*, Available through anonymous ftp at elib.zib-berlin.de in pub/elib/codelib.

Marsden, J.E. [1992], *Lectures on Mechanics* London Mathematical Society Lecture note series, **174**, Cambridge University Press.

Marsden, J.E. and J. Scheurle [1993a] Lagrangian reduction and the double spherical pendulum, *ZAMP* **44**, 17–43.

Marsden, J.E. and J. Scheurle [1993b] The reduced Euler-Lagrange equations, *Fields Institute Comm.* **1**, 139–164.

Marsden, J.E. and J. Scheurle [1995] Pattern evocation and geometric phases in mechanical systems with symmetry, *Dyn. and Stab. of Systems.* (to appear).

McLaughlin, R.I. and C. Scovel [1995] Equivariant constrained symplectic integration. *J. of Nonl. Sci.* **5**, 233–256.

Melbourne, I., M. Dellnitz, and M. Golubitsky [1993] The structure of symmetric attractors. *Arch. Rat. Mech. and An.* **123**, 75–98.

Simo, J.C. and O. Gonzalez [1993] Assessment of energy-momentum and symplectic schemes for stiff dynamical systems. *ASME Winter Annual Meeting*, New Orleans.

Simo, J.C. and N. Tarnow [1992] The discrete energy-momentum method. Conserving algorithms for nonlinear elastodynamics, *ZAMP* **43**, 757–792.

Tarnow, N. [1993] Energy-momentum Conserving Algorithms for Hamiltonian Systems in the Nonlinear Dynamics of Solids *Thesis, Stanford University* **11**, 123–223.

Wendlandt, J.M. [1995] *Pattern Evocation and Energy-Momentum Integration of the Double Sperhical Pendulum.* MA Thesis, Mathematics, UC Berkeley.